

# Magnetic moment and magnetic anisotropy of linear and zigzag 4d and 5d transition metal nanowires: First-principles calculations

J. C. Tung<sup>1</sup> and G. Y. Guo<sup>1,2\*</sup>

<sup>1</sup>*Department of Physics and Center for Theoretical Sciences,  
National Taiwan University, Taipei 106, Taiwan*

<sup>2</sup>*Graduate Institute of Applied Physics, National Chengchi University, Taipei 116, Taiwan  
(Dated: November 1, 2018)*

An extensive *ab initio* study of the physical properties of both linear and zigzag atomic chains of all 4d and 5d transition metals (TM) within the generalized gradient approximation by using the accurate projector-augmented wave method, has been carried out. The atomic structures of equilibrium and metastable states were theoretically determined. All the TM linear chains are found to be unstable against the corresponding zigzag structures. All the TM chains, except Nb, Ag and La, have a stable (or metastable) magnetic state in either the linear or zigzag or both structures. Magnetic states appear also in the sufficiently stretched Nb and La linear chains and in the largely compressed Y and La chains. The spin magnetic moments in the Mo, Tc, Ru, Rh, W, Re chains could be large ( $\geq 1.0 \mu_B/\text{atom}$ ). Structural transformation from the linear to zigzag chains could suppress the magnetism already in the linear chain, induce the magnetism in the zigzag structure, and also cause a change of the magnetic state (ferromagnetic to antiferromagnetic or vice versa). The calculations including the spin-orbit coupling reveal that the orbital moments in the Zr, Tc, Ru, Rh, Pd, Hf, Ta, W, Re, Os, Ir and Pt chains could be rather large ( $\geq 0.1 \mu_B/\text{atom}$ ). Importantly, large magnetic anisotropy energy ( $\geq 1.0 \text{ meV}/\text{atom}$ ) is found in most of the magnetic TM chains, suggesting that these nanowires could have fascinating applications in ultrahigh density magnetic memories and hard disks. In particular, giant magnetic anisotropy energy ( $\geq 10.0 \text{ meV}/\text{atom}$ ) could appear in the Ru, Re, Rh, and Ir chains. Furthermore, the magnetic anisotropy energy in several elongated linear chains could be as large as  $40.0 \text{ meV}/\text{atom}$ . A spin-reorientation transition occurs in the Ru, Ir, Ta, Zr, La and Zr, Ru, La, Ta and Ir linear chains when they are elongated. Remarkably, all the 5d as well as Tc and Pd chains show the colossal magnetic anisotropy (i.e., it is impossible to rotate magnetization into certain directions). Finally, the electronic band structure and density of states of the nanowires have also been calculated in order to understand the electronic origin of the large magnetic anisotropy and orbital magnetic moment as well as to estimate the conduction electron spin polarization.

PACS numbers: 73.63.Nm, 75.30.Gw, 75.75.+a, 61.46.-w

## I. INTRODUCTION

Magnetism in nanostructures has been a very active research area in the last decades<sup>1-4</sup>, because of its novel fundamental physics and fascinating potential applications. Experimentally, modern methods of preparing metal nanowires have made it possible to investigate the influence of dimensionality on the magnetic properties. For example, Gambardella, *et al.*<sup>4</sup>, recently succeeded in preparing a high density of parallel atomic chains along steps by growing Co on a high-purity Pt (997) vicinal surface and also observed one-dimensional (1D) magnetism in a narrow temperature range of 10~20 K. In the mean time, Li, *et al.*<sup>5</sup> reported that Fe stripes on the stepped Pd(110) substrate have a different magnetic easy axis than previous results. Structurally stable nanowires can also be grown inside tubular structures, such as the Ag nanowires of micrometer lengths grown inside self-assembled organic (calix[4]hydroquinone) nanotubes<sup>6</sup>. Short suspended nanowires have been produced by driv-

ing the tip of scanning tunneling microscope into contact with a metallic surface and subsequent retraction, leading to the extrusion of a limited number of atoms from either tip or substrate<sup>7</sup>. Monostrand nanowires of Co and Pd have also been prepared in mechanical break junctions, and full spin-polarized conductance was observed<sup>8</sup>.

Theoretically, a great deal of research has been done on both finite and infinite chains of metal atoms. Theoretical calculations at either semi-empirical tight-binding or *ab initio* density functional theory level for many infinite/finite chains, e.g., linear chains of Co<sup>9-13</sup>, Fe<sup>11,14</sup>, Ni, Pd<sup>15,16</sup>, Pt, Cu<sup>9</sup>, Ag<sup>17,18</sup>, and Au<sup>17,19-22</sup>, as well as zigzag chains of Fe<sup>14</sup>, Zr<sup>23</sup> and Au<sup>21</sup>, have been reported. Early studies of infinite linear chains of Au<sup>21,22,24,25</sup>, Cu<sup>18</sup>, and Pd<sup>20</sup> have shown a wide variety of stable and metastable structures. Recently, the magnetic properties of transition metal infinite linear chains of Fe, Co, Ni, have been calculated<sup>10,11,13,14,26</sup>. Possible magnetism in *s*- and *sp*-electron element linear and zigzag chains have also been studied theoretically.<sup>27</sup> These calculations show that the metallic and magnetic nanowires may become important for electronic/optoelectronic devices, quantum devices, magnetic storage, nanoprobe and spintronics.

Despite of the above mentioned intensive theoretical

\*E-mail: gyguo@phys.ntu.edu.tw

and experimental research, current understanding on the intriguing magnetic properties of nanowires and how magnetism depends their structural property is still incomplete. The purpose of the present work is to make a systematic *ab initio* study of the magnetic, electronic and structural properties of linear and zigzag atomic chains (Fig. 1) of all 4*d* and 5*d* transition metals (TM). Transition metals, because of their partly filled *d* orbitals, have a strong tendency to magnetize. Nonetheless, only 3*d* transition metals (Cr, Mn, Fe, Co, and Ni) exhibit magnetism in their bulk structures. It is, therefore, of interest to investigate possible ferromagnetic (FM) and antiferromagnetic (AF) magnetization in the linear chains of all 4*d* and 5*d* transition metals including Y, Zr, Nb, La, Hf and Ta zigzag chain which appear not to have been considered. As mentioned before, recent *ab initio* calculations indicate that the zigzag chain structure of, at least, Zr<sup>23</sup>, Ir<sup>16</sup>, Pt<sup>16</sup> and Au<sup>16,25</sup>, is energetically more favorable than the linear chain structure. Thus, we also study the structural, electronic and magnetic properties of all 4*d* and 5*d* transition metal zigzag chains in order to understand how the physical properties of the monoatomic chains evolve as their structures change from the linear to zigzag chain.

Relativistic electron spin-orbit coupling (SOC) is the fundamental cause of the orbital magnetization and also the magnetocrystalline anisotropy energy (MAE) of solids. The MAE of a magnetic solid is the difference in total electronic energy between two magnetization directions, or the energy required to rotate the magnetization from one direction to another. It determines whether a magnet is a hard or soft one. Furthermore, it acts to reduce the magnitude of superparamagnetic fluctuation in nanostructures, and hence is a key factor that would determine whether the nanowires have potential applications in, e.g., high-density recording and magnetic memory devices. *Ab initio* calculations of the MAE have been performed for mainly the Fe and Co linear chains<sup>10,28–30</sup>, while semiempirical tight-binding calculations have been reported for both linear chains and two-leg ladders of Fe and Co<sup>30–32</sup>. Very recently, we have carried out systematic *ab initio* calculations of both the MAE and also the magnetic dipolar (shape) anisotropy energy for all 3*d* transition metals in both the linear and zigzag structures.<sup>33</sup> Remarkably, although the SOC is rather weak in 3*d* transition metals, compared with 4*d* and 5*d* transition metals, we found that the FM Ni linear chain has a gigantic MAE of  $\sim 12$  meV/atom.<sup>33</sup> Therefore, as a continuing endeavor to find nanowires with a large MAE, we have calculated the MAE and the magnetic dipolar (shape) anisotropy energy for all 4*d* and 5*d* transition metals in both the linear and zigzag structures. Although in this paper we study only free-standing 4*d* and 5*d* transition metal chains, the underlying physical trends found may also hold for monoatomic nanowires created transiently in break junctions<sup>8</sup> or encapsulated inside 1D nanotubes<sup>6,29</sup> or deposited on weakly interacting substrates<sup>34</sup>, *albeit*, with the actual values of the

physical quantities being modified.

The rest of this paper is organized as follows. In the next section, we briefly describe the theory and computational details we used. The calculated structural and magnetic properties as well as band structures of the linear 4*d* and 5*d* transition metal chains are presented in Sec. III. The calculated structural, magnetic and electronic properties of the zigzag 4*d* and 5*d* transition metal chains in both equilibrium and local energy minimum states are reported in Sec. IV. The relative stability of the linear and zigzag chain structures is analyzed in Sec. V. The calculated magnetic anisotropy energies and moments of both linear and zigzag chains are presented, and also discussed in terms of the calculated *d*-orbital-decomposed DOSs in Sec. VI. Finally, a summary is given in Sec. VII.

## II. THEORY AND COMPUTATIONAL METHOD

In the present calculations, we use the accurate frozen-core full-potential projector augmented-wave (PAW) method,<sup>35</sup> as implemented in the Vienna *ab initio* simulation package (VASP)<sup>36,37</sup>. The calculations are based on density functional theory with the generalized gradient approximation (GGA)<sup>38</sup>. The free-standing atomic chains are modelled by a two-dimensional array of infinite long, straight or zigzag wires. For both linear and zigzag chains, the nearest wire-wire distance between the neighboring chains is, at least, 15 Å, which should be wide enough to decouple the neighboring wires. A large plane-wave cutoff energy of  $\sim 350$  eV is used for all 4*d* and 5*d* transition metal chains.

The equilibrium bond length (lattice constant) of the linear atomic chains in the nonmagnetic (NM), ferromagnetic (FM) and antiferromagnetic (AF) states is determined by locating the minimum in the calculated total energy as a function of the interatomic distance. The results are also compared with that obtained by structural optimizations, and the differences are small (within 0.4 %) for, e.g., the Ru, Rh and Pd chains. For the zigzag chains, the theoretical atomic structure is determined by structural relaxations using the conjugate gradient method. The equilibrium structure is obtained when all the forces acting on the atoms and the axial stress are less than 0.02 eV/Å and 2.0 kBar, respectively. The  $\Gamma$ -centered Monkhorst-Pack scheme with a *k*-mesh of  $1 \times 1 \times n$  ( $n = 40$ ) in the full Brillouin zone (BZ), in conjunction with the Fermi-Dirac-smearing method with  $\sigma = 0.01$  eV, is used to generate *k*-points for the BZ integration. With this *k*-point mesh, the total energy is found to converge to within  $10^{-3}$  eV.

Because of its smallness, *ab initio* calculation of the MAE is computationally very demanding and needs to be carefully carried out (see, e.g., Refs. 39,40). A very fine *k*-point mesh with *n* being 200 for both the linear and zigzag chains, is used. The same *k*-point mesh is used for

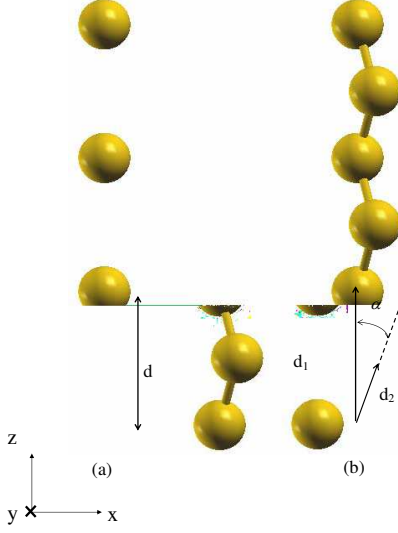


FIG. 1: (color online) Schematic structure diagram for (a) the linear and (b) zigzag atomic chains.

the band structure and density of states calculations. As in our previous publication on the 3d TM chains<sup>33</sup>, we use the force theorem approach to calculate the MAE, i.e., the MAE is calculated as the total energy difference between the two relativistic band structure calculations for the two different magnetization directions (e.g., parallel and perpendicular to the chain) concerned using the frozen charge density obtained in a prior self-consistent scalar relativistic calculation.<sup>41</sup> The total energy convergence criteria is  $10^{-7}$  eV/atom.

### III. LINEAR CHAINS

#### A. Magnetic state and spin magnetic moment

The calculated equilibrium bond lengths ( $d$ ) and spin magnetic moments of all the 4d and 5d transition metal linear chains in the NM, FM and AF states are displayed in Fig. 2, and Fig. 3, respectively. They are also listed in Table I. The calculated total energy relative to that of the NM state (i.e., the magnetization energy) of the FM and AF linear atomic chains are also shown in Fig. 2, Fig. 3 and Table I. It is clear from Figs. 2 and 3 that all of the 4d and 5d TM elements except Y, Nb, La, Ta, Os and Pt, become magnetic in the linear chain structure. Furthermore, for all the 4d and 5d TM elements, except Y, Nb, La, Ta, Os and Pt, NM state is unstable and the ground state is either FM and AF (see Fig. 2, Fig. 3 and Table I). Among the 4d TM linear chains, the ground state for the Zr, Ru, Rh, and Pd chains is ferromagnetic while that for the Mo, and Tc chains is antiferromag-

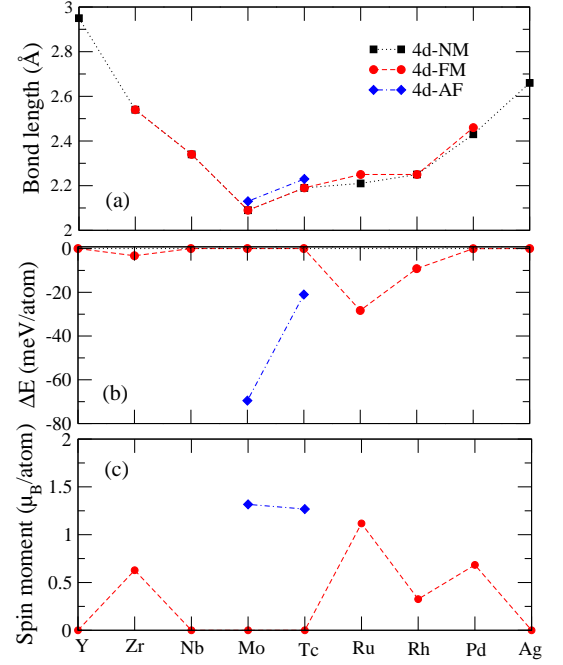


FIG. 2: (color online) (a) Equilibrium bond length ( $\text{\AA}$ ), (b) magnetization energy ( $\Delta E$ ) (i.e., the total energy of a magnetic state relative to that of nonmagnetic state) ( $\Delta E = E^{FM(AF)} - E^{NM}$ ) and (c) spin magnetic moments ( $\mu_B$ ) of all the 4d TM linear atomic chains in the NM, FM, and AF states.

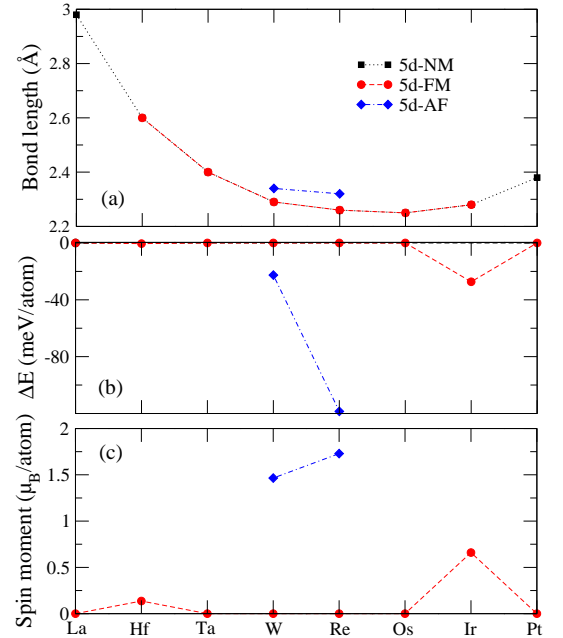


FIG. 3: (color online) (a) Equilibrium bond length ( $\text{\AA}$ ), (b) magnetization energy ( $\Delta E$ ) (i.e., the total energy of a magnetic state relative to that of nonmagnetic state) ( $\Delta E = E^{FM(AF)} - E^{NM}$ ) and (c) spin magnetic moments ( $\mu_B$ ) of all the 5d TM linear atomic chains in the NM, FM, and AF states.

netic. For the  $5d$  TM linear chains, the ground state for the Hf and Ir chains is ferromagnetic and the ground state for the Re and W are antiferromagnetic. The Y, Nb, La, Ta, Os and Pt chains are nonmagnetic at the equilibrium bond length. We recently reported<sup>33</sup> that in the  $3d$  TM linear chains, the equilibrium bond length in a magnetic state is significantly larger than that in the nonmagnetic state. For example, the magnetization induced increase in the bond length in the Cr chain is 54 %. In contrast, Fig. 2, Fig. 3 and Table I show that in the  $4d$  and  $5d$  TM linear chains, the difference in bond length between a magnetic (FM or AF) state and the NM state is much smaller. The largest lattice magnetolattice expansion occurs in the AF Re chain but it amounts only to 3 %. This is due to much weak magnetization in the  $4d$  and  $5d$  linear chains, as indicated by the smaller magnetic moments and much smaller magnetization energies in these atomic chains at equilibrium (Table I).

To see how the magnetic properties of the atomic chains evolve with the interatomic distance, we plot the spin and orbital moments for some  $4d$  (Y, Zr, Nb, and Pd) and  $5d$  (La, Hf, Ta, Os, Ir and Pt) TM chains in the FM state as a function of the bond length in Fig. 4. For most selected ferromagnetic TM (except Y, La, Zr and Hf) chains, the spin moment generally becomes larger as the bond length is increased from its equilibrium value (Table I). Interestingly, the spin moment of the Hf chain, in contrast, decreases monotonically when the chain is elongated, and eventually disappears at the bond length of 2.7 Å [Fig. 4(c)]. The spin moment of the Zr chain decreases slightly as the bond length increases, but increases again when the bond length goes beyond  $\sim 2.7$  Å. Surprisingly, when the Y (La) chain is sufficiently compressed [at the bond length of  $\sim 2.35$  (2.65) Å], the ferromagnetism appears, and the spin moment increases as the chain is further compressed. Finally, for the Y, La, Ta, Os and Pt chains, the sufficient elongation of the bond length would induce a FM state (Fig. 4).

Our calculated bond lengths, spin moments and magnetization energies generally agree rather well with available previous *ab initio* calculations<sup>15,20,26,29,42–44</sup>. Nonetheless, a few notable differences exist. For example, our calculated bond length (2.13 Å) of the AF Mo chain is 7.0 % smaller than that (2.28 Å) reported in Ref. 44 but in good agreement with Ref. 15 (2.15 Å). Also, our equilibrium bond lengths of the Os and Pt chains are smaller than that from Ref 20, but the differences are within 2.7 %. Another notable difference is that our calculations suggest that the Os chain is nonmagnetic in equilibrium but become ferromagnetic only when the bond length is larger than  $\sim 2.55$  Å (Fig. 4), while, according to Ref. 20, it is ferromagnetic at the equilibrium bond length. Our calculated magnetization energies (Table I) for the AF Mo and Tc chains are smaller than that reported in Ref. 44 (197 and 53 meV/atom, respectively) and in Ref. 15 (92 and 65 meV/atom, respectively).

TABLE I: Equilibrium bond lengths ( $d$ ) (in Å), total energies ( $E_t$ ) (in meV/atom) in the FM and AF states (relative to the NM state), and spin magnetic moments ( $m_s$ ) (in  $\mu_B$ /atom), of the  $4d$  and  $5d$  transition metal linear chains from scalar relativistic calculations.

	$d_{NM}$	$E_t^{FM}$	$m_s^{FM}$	$d_{FM}$	$E_t^{AF}$	$m_s^{AF}$	$d_{AF}$
4d metals							
Y	2.95						
Zr	2.54	-3.29	0.628	2.54			
Nb	2.34						
Mo	2.09				-69.53	1.317	2.13
Tc	2.19				-21.02	1.268	2.23
Ru	2.21	-28.30	1.118	2.25			
Rh	2.25	-9.19	0.328	2.25			
Pd	2.43	-0.05	0.684	2.46			
Ag	2.66						
5d metals							
La	2.98						
Hf	2.60	-0.46	0.137	2.60			
Ta	2.40						
W	2.29				-22.59	1.465	2.34
Re	2.26				-118.52	1.729	2.32
Os	2.25						
Ir	2.28	-27.32	0.660	2.28			
Pt	2.38						
Au	2.60						

TABLE II: Spin ( $m_s$ ) and orbital ( $m_o$ ) magnetic moments (in  $\mu_B$ /atom) of the magnetic  $4d$  and  $5d$  transition metal linear chains at the equilibrium bond lengths (Table I) with magnetization parallel ( $\mathbf{m} \parallel \hat{z}$ ) and perpendicular ( $\mathbf{m} \perp \hat{z}$ ) to the chain axis from fully relativistic charge selfconsistent calculations.

		$\mathbf{m} \parallel \hat{z}$		$\mathbf{m} \perp \hat{z}$	
		$m_s$	$m_o$	$m_s$	$m_o$
4d metals					
Zr	(FM)	0.631	-0.065	0.610	-0.007
Mo	(AF)	1.337	-0.008	1.181	0.005
Tc	(AF)	1.353	0.463	1.252	0.046
Ru	(FM)	1.115	-0.106	1.076	0.058
Rh	(FM)	0.317	0.428	0.017	0.000
Pd	(FM)	0.345	-0.043	0.636	0.126
5d metals					
Hf	(FM)	0.235	-0.198		
W	(AF)	1.184	-0.307	1.371	-0.005
Re	(AF)	1.564	0.115	1.644	0.146
Os	(FM)			0.444	0.046
Pt	2.38	0.124	0.100		

## B. Orbital magnetic moment and colossal magnetic anisotropy

The spin and orbital magnetic moments in the magnetic  $4d$  and  $5d$  TM atomic chains in equilibrium from the fully relativistic charge selfconsistent calculations are listed in Table II. We note that the SOC affect slightly the spin moments in the AF TM chains and also FM Zr and Ru chains (see Tables I and II). However, in the other

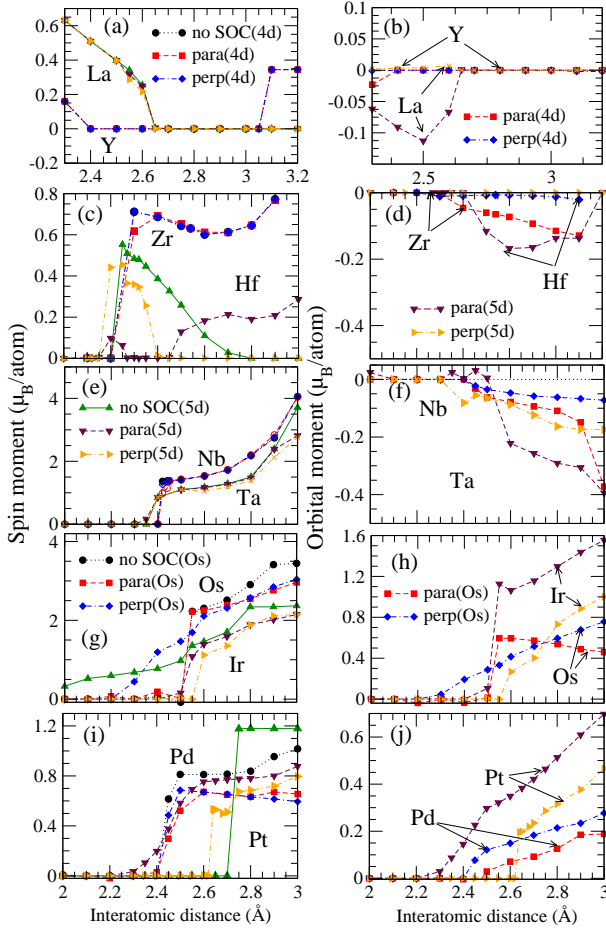


FIG. 4: (color online) Spin (left panels) and orbital (right panels) magnetic moments as a function of interatomic distance of the ferromagnetic Y, La, Zr, Hf, Nb, Ta, Os, Ir, Pd and Pt linear chains. In the left panels, "no-SOC" means the results from the scalar relativistic calculations. "Para" ("perp") denotes the magnetization being parallel (perpendicular) to the chain axis. The spin magnetic moment for the Pd chain goes to zero at  $\sim 3.6$  Å.

cases, the spin magnetic moments in Table II are generally much smaller than that obtained from the scalar-relativistic calculations (Table I), unlike in the  $3d$  TM chains where the SOC hardly affects the spin magnetic moments<sup>33</sup>. In fact, the SOC completely suppresses the spin magnetic moment in the FM Ir chain in equilibrium (Tables I and II). Interestingly, the SOC-induced reduction of the spin magnetic moment is magnetization-direction dependent. Table II shows that the spin moment of the Rh chain with magnetization parallel to the chain axis remains almost unchanged while that perpendicular to the axis becomes nearly diminished. In the Pd chain, in contrast, the spin moment for magnetization along the axis decreases nearly by half while that perpendicular to the axis remains nearly unchanged (Table II). Dramatically, in the FM Hf chain, the SOC fully suppresses the magnetization when the magnetization is perpendicular to the chain axis, but it nearly doubles the

spin moment when the magnetization is along the axis. This interesting magnetic anisotropy is called the colossal magnetic anisotropy (CMA) by Smogunov *et al.*<sup>45</sup>, who reported recently this CMA in the Pt chain. The CMA means that a magnetization magnitude could be finite only along certain directions and also that it is strictly impossible to rotate magnetization into certain directions. Earlier calculations<sup>44</sup> also suggested the CMA to occur in the Rh linear chain. Our calculations here not only corroborate this finding of Smogunov *et al.*<sup>45</sup> but also reveal the CMA in other  $5d$  transition metal linear chains such as Hf and Os (Table II).

When the SOC is not taken into account, the spin moment in the  $4d$  and  $5d$  TM linear chains generally increases monotonically as the bond length is increased, as shown in Fig. 4. However, the behavior of the magnetic properties of the  $5d$  TM linear chains under the influence of the SOC is very different from that of the  $3d$  TM chains. For example, from the scalar relativistic calculations, the Ir chain at the interatomic distance starting from 2.0 to 3.0 Å, has a finite magnetic moment in the range of  $0.4 \sim 2.4 \mu_B/\text{atom}$  (Fig. 4g). When the SOC is taken into account, the Ir chain becomes nonmagnetic when the interatomic distance is smaller than 2.5 Å, but has a finite magnetic moment when the interatomic distance larger than 2.5 Å. Similar behavior can also be seen in the Os, and Pt chains (Fig. 4g and i). Our scalar relativistic calculations show that the Os chain is nonmagnetic if the interatomic distance is below 2.4 Å, whilst our fully relativistic calculations indicate that, for the magnetization perpendicular to the chain direction, it becomes magnetic at the interatomic distance above 2.2 Å. In contrast, for the axial magnetization, the Os chain would become ferromagnetic only when the interatomic distance is larger than 2.5 Å. Therefore, the Os chain exhibits the CMA<sup>45</sup> when the interatomic distance falls between 2.2 and 2.5 Å. Fig. 4 further shows that the Hf, Ir and Pt linear chains also exhibit the CMA in the interatomic distance of  $2.25 \sim 3.0$  Å (Hf),  $2.52 \sim 2.78$  Å (Ir) and  $2.30 \sim 2.63$  Å (Pt), respectively.

The SOC provides the essential symmetry breaking that gives rise to orbital magnetization in magnetic solids. When the SOC is included in our calculations, the calculated orbital magnetic moments in the FM  $4d$  TM chains at equilibrium bond length are listed in Table II. Surprisingly, even for the  $5d$  TM linear atomic chains, the calculated orbital magnetic moments are not large. For example, the calculated orbital moments in the  $5d$  TM linear atomic chains are within  $\sim 0.2 \mu_B/\text{atom}$  (Table II). The calculated orbital moments in the  $4d$  TM linear chains in equilibrium can be larger, e.g., being  $\sim 0.2 \mu_B/\text{atom}$  in the AF Tc and FM Rh chains with the magnetization along the chain direction (Table II), respectively. Therefore, although the SOC is stronger in  $4d$  and  $5d$  transition metals than in  $3d$  ones, the calculated orbital magnetic moments in the  $4d$  and  $5d$  transition metals chains at the equilibrium bondlength is not necessarily larger than in the  $3d$  transition metal chains.<sup>33</sup> As

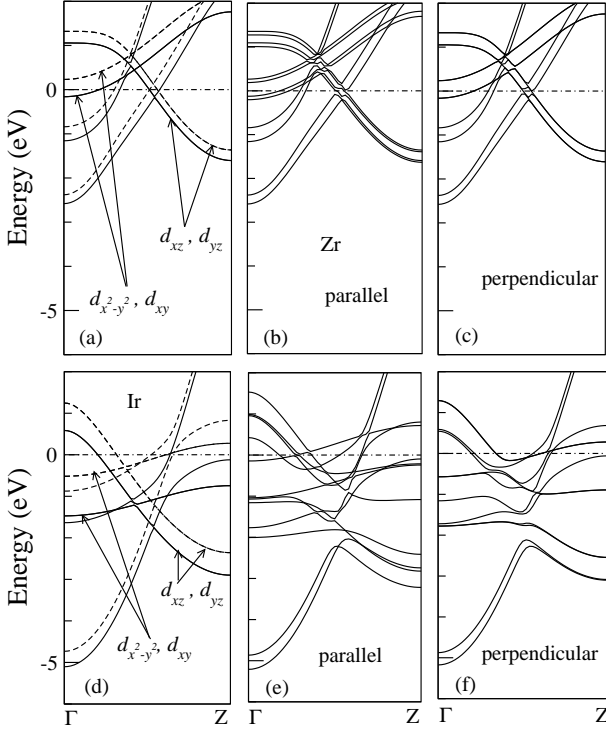


FIG. 5: Band structures of the Zr (upper panels) and Ir (lower panels) linear chains at 2.6 Å. Left panels: the scalar-relativistic band structures; the middle and right panels: the fully relativistic band structures with the magnetization parallel to and perpendicular to the chain axis, respectively. In the left panels, the solid and dashed lines represent (spin up) and (spin down) bands, respectively. The Fermi level (the dotted horizontal line) is at the zero energy.

for the spin moments, the magnitude of the orbital moments generally increases monotonically with the bond length, as can be seen in Fig. 4, with one notable exception of the La chain (Fig. 4b). The orbital moment shows a strong dependence on the magnetization orientation (Fig. 4, right panels). As in the 3d TM chains<sup>33</sup>, the orbital moment in the 4d and 5d TM chains with the magnetization along the chain direction is usually much higher than that for the magnetization perpendicular to the chain. However, in the Pd chain, the orbital moment with the magnetization along the chain direction is significantly larger than that for the magnetization perpendicular to the chain. (Fig. 4j).

### C. Band structures and density of states

Let us now examine the band structure of selected transition metal linear chains in order to understand the calculated magnetic properties. The energy bands obtained without and also with the SOC for the Zr and Ir chains in the FM state at 2.6 Å are plotted in Fig. 5. In the absence of the SOC, because of the uniaxial rotational symmetry, the bands may be grouped into three sets,

namely, the nondegenerate  $s$ - and  $d_{z^2}$ -dominant bands, double degenerate  $(d_{xz}, d_{yz})$ , and  $(d_{x^2-y^2}, d_{xy})$  dominant bands (see the left panels in Fig. 5). The  $(d_{x^2-y^2}, d_{xy})$  bands are narrow because the  $d_{x^2-y^2}$  and  $d_{xy}$  orbitals are perpendicular to the chain, thus forming weak  $\delta$  bonds. The  $(d_{xz}, d_{yz})$  bands, on the other hands, are more dispersive due to the stronger overlap of the  $d_{xz}$  and  $d_{yz}$  orbitals along the chain, which gives rise to the  $\pi$  bonds. The  $s$ - and  $d_{z^2}$  dominant bands are most dispersive since these orbitals form strong  $\sigma$  bonds along the chain. The left panels in Fig. 5 show that the less dispersive  $d_{x^2-y^2}, d_{xy}$  bands are near the Fermi level and spin-split. In the Zr linear chain, one spin-split  $d_{x^2-y^2}, d_{xy}$  band is partially occupied near the  $\Gamma$ -point while the other band is completely empty. In the Ir chain, one split band lies completely below the Fermi level while the other band is only partially occupied. Thus, the relatively narrow  $d_{x^2-y^2}, d_{xy}$  bands play an important role in magnetism, and that is the main reason why Zr and Ir chains are ferromagnetic at the bondlength of 2.6 Å.

The directional dependence of the orbital magnetization can be explained by analyzing the fully relativistic band structures (see Fig. 5). For the Zr linear chain with the axial magnetization (Fig. 5b), the doubly degenerate  $d_{x^2-y^2}, d_{xy}$  bands are split into two with angular momenta  $m_l = \pm 2$ . If one of them is fully occupied and the other is empty, the resulting orbital moment is 2. Nonetheless, in the Zr linear chain, both are partially occupied with different occupation numbers (Fig. 5b), resulting in an orbital moment of  $-0.07 \mu_B/\text{atom}$ . Of course, the larger the SOC splitting, the larger the difference in the occupation number and hence the larger the orbital moment. Therefore, the Ir chain has a larger axial orbital moment ( $1.06 \mu_B/\text{atom}$ ), because one of the split  $d_{x^2-y^2}, d_{xy}$  bands lies almost completely below the Fermi level (see Fig. 5e). However, for the perpendicular magnetization, the  $d_{x^2-y^2}, d_{xy}$  bands remain degenerate (Fig. 5c and Fig. 5f) and hence do not contribute to the orbital magnetization. Nonetheless, as pointed out in Ref. 44, the SO-split  $d_{x^2-y^2}, d_{xy}$ - $(d_{xz}, d_{yz})$  bands near the Fermi level would hybridize (Fig. 5f) and this hybridization would give rise to a smaller perpendicular orbital moment of  $0.27 \mu_B/\text{atom}$  in the Ir linear chain. For the Zr chain, this hybridization does not occur near the Fermi energy (Fig. 5c). Therefore, the Zr chain have a tiny orbital moment of  $-0.01 \mu_B/\text{atom}$  when the magnetization is perpendicular to the chain axis. Of course, when the SOC is included, the degenerate  $d_{xz}, d_{yz}$  bands are also split into the  $m_l = -1$  and  $+1$  bands for the axial magnetization, but remain degenerate for the perpendicular magnetization (see Fig. 5). This SOC splitting of the  $(d_{xz}, d_{yz})$  band and  $(d_{x^2-y^2}, d_{xy})$  band is proportional to  $|\langle d_{xz} | H_{SO} | d_{yz} \rangle|^2$  and  $|\langle d_{x^2-y^2} | H_{SO} | d_{xy} \rangle|^2$ , respectively. Here  $H_{SO}$  is the SOC Hamiltonian. Since  $|\langle d_{xz} | H_{SO} | d_{yz} \rangle|^2 : |\langle d_{x^2-y^2} | H_{SO} | d_{xy} \rangle|^2 = 1:4$ ,<sup>46</sup> the SOC splitting of the  $(d_{xz}, d_{yz})$  bands is much smaller than the  $(d_{x^2-y^2}, d_{xy})$  bands (see Fig. 5). Therefore, the  $(d_{xz}, d_{yz})$  bands would make a much smaller contribution

TABLE III: Numbers ( $n_c^\uparrow$  and  $n_c^\downarrow$ ) of the spin-up and spin-down conduction bands crossing the Fermi level, and spin-polarization  $P$  at the Fermi level for the  $4d$  and  $5d$  TM atomic chains in the FM state.

linear chain		zigzag chain	
$(n_c^\uparrow, n_c^\downarrow)$	$P$	$(n_c^\uparrow, n_c^\downarrow)$	$P$
<i>4d</i> metals			
Y		(2,3)	0.09
Zr	(4,3)	(3,4)	-0.09
Mo		(6,8)	-0.11
Ru	(3,4)		
Rh	(3,4)	(3,6)	-0.53
Pd	(3,4)	(3,6)	-0.30
<i>5d</i> metals			
Hf	(4,3)		
W		(6,8)	-0.16
Re		(2,4)	-0.38
Os		(5,7)	-0.10
Ir	(3,4)	(7,9)	-0.28

to the orbital magnetization

Electric and spin current transports are determined by the characteristics of the band structure near the Fermi level ( $E_F$ ) in the systems concerned. Therefore, it would be interesting to examine the energy bands and density of states (DOS) of the atomic chains in the vicinity of the  $E_F$ . The spin-decomposed DOS for all the  $4d$  and  $5d$  linear chains in equilibrium are displayed in Fig. 7 and Fig. 8, respectively. For the FM Zr, Ru, Rh, Pd, Hf and Ir chains, the density of states at the  $E_F$  are spin-polarized (Fig. 7 and Fig. 8). This is usually quantified by the spin-polarization  $P$  defined as

$$P = \frac{N_\uparrow(E_F) - N_\downarrow(E_F)}{N_\uparrow(E_F) + N_\downarrow(E_F)}, \quad (1)$$

where  $N_\uparrow(E_F)$  and  $N_\downarrow(E_F)$  are the spin-up and spin-down DOS at the  $E_F$ , respectively. The most useful materials for the spintronic applications are the so-called half-metallic materials in which one spin channel is metallic and the other spin channel is insulating. The spin-polarization for these half-metals is either 1.0 or -1.0, and the electric conduction would be fully spin-polarized. The calculated spin-polarization and also the numbers of the conduction bands that cross the Fermi level in the  $4d$  and  $5d$  TM chains are listed in Table III. It is clear that the  $P$  of the FM Zr, Ru, Rh, and Ir linear chains is rather large ( $\geq 0.4$ ), though still smaller than many  $3d$  TM linear chains.<sup>33</sup> None of the  $4d$  and  $5d$  TM linear chains in the FM state is half-metallic. Interestingly, the FM Zr chain has a positive spin polarization, while the Ru, Rh, Hf, Pd and Ir chains have a negative spin polarization (Table II, Fig. 7 and Fig. 8).

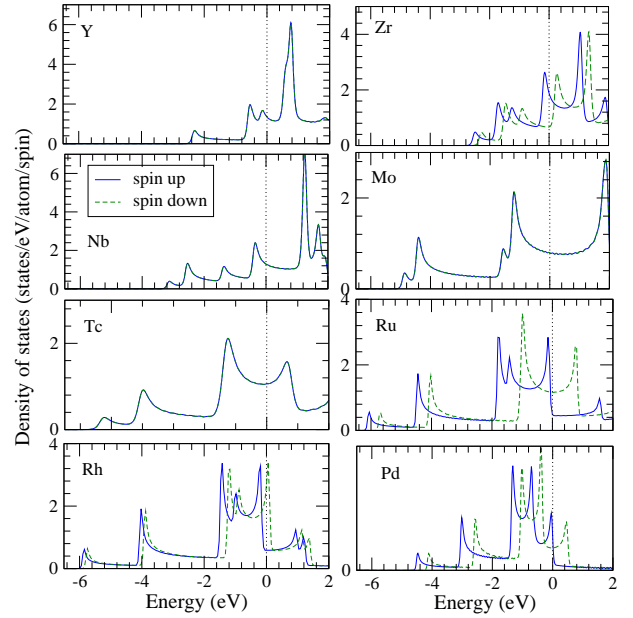


FIG. 6: (color online) Density of states of the FM  $4d$  TM linear atomic chains at the equilibrium bond length. The Fermi level (dotted vertical lines) is at the zero energy.

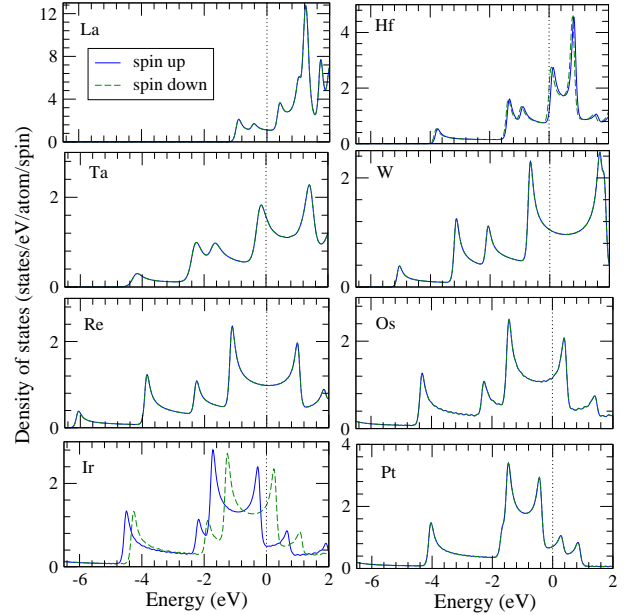


FIG. 7: (color online) Density of states of the FM  $5d$  TM linear atomic chains at the equilibrium bond length. The Fermi level (dotted vertical lines) is at the zero energy.

#### IV. ZIGZAG CHAINS

The zigzag structure for metal monoatomic wires has already been observed in experiments<sup>47</sup>. Among  $4d$  and  $5d$  transition metals, structural<sup>17,23</sup> and magnetic<sup>16</sup> properties of Zr, Rh, Pd, W, Ir, and Pt zigzag atomic chains have been studied theoretically in recent years.



TABLE IV: Equilibrium structural parameters (see Fig. 1b for symbols  $d_1$ ,  $d_2$ ,  $\alpha$ ), spin magnetic moment ( $m_s$ ) and magnetization energy ( $\Delta E$ ) of the 4d and 5d transition metal zigzag chains from the scalar relativistic calculations.  $d_1$  and  $d_2$  are in the unit of Å, and  $\alpha$  is in the unit of degree.  $\Delta E$  is in the unit of meV/atom, and  $m_s$  in the unit of  $\mu_B$ /atom.

		$d_1$	$d_2$	$\alpha$	$m_s$	$\Delta E$
4d metals						
Y	(NM)	3.12	3.03	59.0		
	(FM)	3.17	3.08	59.0	0.482	388.1
Zr	(NM)	2.81	2.71	58.7		
	(FM)	2.85	2.74	58.6	0.162	-2.93
Nb	(NM)	2.51	2.63	61.5		
Mo	(NM)	2.38	2.51	61.7		
	(FM)	2.45	2.53	61.0	0.267	-2.90
Tc	(NM)	2.40	2.47	60.9		
Ru	(NM)	2.40	2.47	60.9		
	(FM)	2.49	2.48	59.5	1.526	-26.0
	(AF)	2.41	2.46	60.7	0.306	-5.9
Rh	(NM)	2.39	2.60	62.6		
	(FM)	2.59	2.49	59.1	1.355	-30.0
Pd	(NM)	2.56	2.64	61.0		
	(FM)	2.55	2.66	61.3	0.392	-0.7
	(AF)	2.56	2.64	60.9	0.266	-2.2
Ag	(NM)	2.73	2.78	60.9		
5d metals						
La	(NM)	3.24	3.10	58.5		
Hf	(NM)	2.89	2.71	57.7		
Ta	(NM)	2.75	2.51	56.7		
W	(NM)	2.48	2.56	61.0		
	(FM)	2.48	2.56	61.0	0.262	-1.8
Re	(NM)	3.22	2.25	48.8		
	(FM)	3.22	2.25	44.3	0.516	-259.5
Os	(NM)	2.49	2.44	59.3		
	(FM)	2.50	2.44	59.1	0.457	-26.7
	(AF)	2.50	2.44	59.2	0.360	-7.9
Ir	(NM)	2.45	2.53	61.0		
	(FM)	2.44	2.56	61.5	0.629	-36.7
Pt	(NM)	2.49	2.65	62.0		
Au	(NM)	2.67	2.76	61.1		

In the present paper, we perform a systematic *ab initio* study of the structural, electronic and magnetic properties of the zigzag chain structure of all the 4d and 5d transition metals.

### A. Structure and magnetic moments

The calculated equilibrium structural parameters (Fig. 1b), spin magnetic moment and magnetization energy of the 4d and 5d TM zigzag chains are listed in Table IV. First of all, Table IV shows that all the zigzag chains except the Re one, look like planar equilateral triangle ribbons, i.e., the two bond lengths  $d_1$  and  $d_2$  are similar and the angle  $\alpha$  is close to  $60^\circ$  (Fig. 1b). The equilibrium bond lengths  $d_1$  and  $d_2$  are generally a few percents larger than the bond length  $d$  of the corresponding linear chains (Table I). This is because the zigzag chains which

TABLE V: Structural parameters ( $d_1$ ,  $d_2$ ,  $\alpha$ ) (see Fig. 1b) of the zigzag chain at the second local energy minimum state.  $d_1$  and  $d_2$  are in the unit of Å, and  $\alpha$  is in the unit of degree.  $\Delta E$  (meV/atom) is the energy difference between the second energy minimum and the corresponding energy minimum listed in Table IV. The second local minimum state of the Zr and Ir chains only is ferromagnetic with a spin moment of 0.295 and 0.285  $\mu_B$ /atom, respectively. The elements whose zigzag chains do not have the second energy minimum are not listed here

		$d_1$	$d_2$	$\alpha$	$\Delta E$
4d metals					
Zr	(FM)	4.25	2.44	29.6	1015
Nb	(NM)	2.80	2.45	55.1	-41.6
Mo	(NM)	3.10	2.24	46.3	-295.7
Tc	(NM)	3.32	2.20	41.1	-24.0
5d metals					
W	(NM)	3.00	2.31	49.6	-127.8
Re	(NM)	3.20	2.21	43.7	-102.6
Ir	(FM)	4.00	2.27	28.4	207.4
Pt	(NM)	4.27	2.37	25.8	412.0
Au	(NM)	4.60	2.55	28.2	330.6

form planar equilateral triangle ribbons, have a higher coordination number (four) than that (two) of the linear chains. Similarly, all these bond lengths are shorter than their counterparts in the bulk structures. For example, the bond lengths for bcc Nb, bcc Mo, fcc Rh, fcc Pd, bcc W, fcc Ir and fcc Pt are, 2.86, 2.73, 2.68, 2.75, 2.86, 2.72 and 2.77 Å, respectively.<sup>48</sup>

Our calculated equilibrium structural parameters ( $d_1$ ,  $d_2$ ,  $\alpha$ ) agree reasonably well with available previous calculations<sup>16,17,23</sup>. For example, Lin *et al.* reported  $d_1 = 2.86$  Å,  $d_2 = 2.74$  Å,  $\alpha = 58.5^\circ$  for the Zr zigzag chain, being consistent with our values in Table IV. Reported parameters  $d_1$ ,  $d_2$ , and  $\alpha$  for the W (2.44, 2.59, 61.9), Os (2.48, 2.56, 61.1), Pt (2.58, 2.73, 61.9) and Au (2.64, 2.73, 61.13) chains (estimated from Figs. 3 and 5 in Ref. 16) are in rather good agreement with our results in Table IV. One exception is the Ir chain<sup>16</sup> where  $d_1 = 2.50$  Å,  $d_2 = 4.53$  Å,  $\alpha = 74.0^\circ$  differs substantially from the present results. Secondly, all the 4d and 5d TM zigzag chains except that of Nb, Tc, La, Hf, Ta and Pt, have magnetic solutions in the equilibrium structures (Table IV). Further, the Zr, Mo, Ru, Rh, W, Re, Os, and Ir zigzag chains are most stable in the FM state, whilst the ground state of the Pd zigzag chain is antiferromagnetic. For comparison, the ground state of the linear Mo, Tc, W and Re chain is antiferromagnetic (Table I). The FM Ru and Rh zigzag chains have a rather large spin moment of  $\sim 1.5 \mu_B$ /atom, though the other magnetic zigzag chains generally have a small spin moment ( $\leq 1.0 \mu_B$ /atom) (Table IV). Interestingly, the ground state of the Y zigzag chain is nonmagnetic, though it has a FM solution with a spin magnetic moment of  $\sim 0.5 \mu_B$ /atom. Note that none of the 4d and 5d TMs is magnetic in their bulk structures in nature. Thirdly, for some 4d and 5d



transition metals, the ground state magnetic configuration changes when the structure changes from the linear to zigzag chain. For example, the Tc and Hf elements are nonmagnetic in their equilibrium zigzag chain structures, though they are, respectively, antiferromagnetic and ferromagnetic in their equilibrium linear chain structures (Table I). This is due to the increase in the coordination number in the zigzag chains because most of them form a planar equilateral triangle ribbon. On the other hand, the Y and Os elements become ferromagnetic in the zigzag chains even though they are nonmagnetic in the linear chains. Finally, the ground state of the Mo, W and Re chains changes from the AF state in the linear chain to the FM state in the zigzag structure.

The  $\text{Zr}^{23}$ ,  $\text{Ru}^{17}$ ,  $\text{Os}$ ,  $\text{Au}^{16}$ ,  $\text{Ir}$  and  $\text{Pt}^{16,55}$  zigzag chains were reported to have a metastable non-triangular elongated zigzag structure with  $\alpha$  being  $\sim 30.0^\circ$ . The existence of this second energy minimum elongated zigzag structure ( $\alpha$  being  $\sim 30.0^\circ$ ) is believed to be crucial to the formation of a transient atomic chain in the break-junction experiments.<sup>16,55</sup> To systematically study these possible elongated zigzag structures, we therefore further calculated the total energy as a function of the fixed lattice constant  $d_1$  with  $d_1$  varying from 2.0 Å to 6.0 Å for all the 4d and 5d zigzag chains. The structural parameters for the second local (or global) energy minimum state of the zigzag chains are listed in Table V. Note that the equilibrium structural parameters listed in Table IV were obtained by unrestricted structural relaxations using the conjugate gradient method (see Sec. II). Our present calculations corroborate some of these previous findings. For example, in the metastable Zr, Ir, Pt and Au chains, we find the angle  $\theta$  to be  $29.6^\circ, 28.4^\circ, 25.8^\circ, 28.2^\circ$ ,  $d_1 = 4.25, 4.00, 4.27, 4.60$  Å, and spin moment  $m_s = 0.30, 0.28, 0.00, 0.00 \mu_B/\text{atom}$ , respectively. In these metastable Zr, Ir, Pt and Au zigzag chains, the total energy is, respectively, 1.02, 0.21, 0.41, 0.33 eV/atom higher than the ground state triangular zigzag chains. However, we don't find a second local (or global) energy minimum state in the Ru and Os zigzag chains, in contrast to the previous studies.<sup>16,17</sup> The discrepancy on the Ru chain between the present and previous<sup>17</sup> studies could be attributed to the fact that highly accurate PAW potential rather than norm-conserving pseudopotential, is used here, while the difference on the Os chain might be caused by the use of the faster but less accurate norm-conserving pseudopotential linear combination of atomic orbitals method in Ref. 16. Surprisingly, the second energy minimum state in the Nb, Mo, Tc, W and Re chains (Table V) is in fact the global energy minimum, i.e., its total energy is below the corresponding minimum energy listed in Table IV. This result for the W chain is in agreement with the previous study of Ref. 16. Moreover, the bondlength  $d_1$  of this second minimum state is not much larger than that of the first minimum state and the angle  $\alpha$  is not close to  $30.0^\circ$ . These results appear to be consistent with the observation that only Ir, Pt and Au could form an atomic chain in the break-junction experiments.

TABLE VI: Spin ( $m_s$ ) and orbital ( $m_o$ ) magnetic moments (in  $\mu_B/\text{atom}$ ) of the magnetic 4d and 5d transition metal zigzag chains in the equilibrium structures (Table IV) with magnetization parallel ( $\mathbf{m} \parallel \hat{z}$ ) and perpendicular ( $\mathbf{m} \parallel \hat{x}$ ,  $\mathbf{m} \parallel \hat{y}$ ) (see Fig. 1) to the chain axis from fully relativistic charge self-consistent calculations. Superscript  $a$  denotes the orbital moments on two neighboring atoms are antiparallel, though the system is in spin ferromagnetic state. Superscript  $\hat{y}$  means that the orbital moment is along the  $y$ -axis, though the spin moment is along the  $x$ -axis, i.e., the spin and orbital moments are noncollinear.

		$\mathbf{m} \parallel \hat{z}$		$\mathbf{m} \parallel \hat{x}$		$\mathbf{m} \parallel \hat{y}$	
		$m_s$	$m_o$	$m_s$	$m_o$	$m_s$	$m_o$
4d metals							
Y	(FM)	0.982	0.004	0.979	0.079 <sup>a, <math>\hat{y}</math></sup>	0.981	0.079 <sup>a</sup>
Zr	(FM)	0.162	-0.003	0.162	0.149 <sup>a, <math>\hat{y}</math></sup>	0.162	-0.002 <sup>a</sup>
Tc	(AF)					0.032	-0.257
Ru	(FM)	1.526	0.151	1.379	0.104	1.452	0.030
	(AF)	0.286	0.144	0.263	0.024	0.261	0.009
Rh	(FM)	1.356	0.338	1.321	0.205	1.321	0.085
Pd	(FM)			0.182	0.045	0.155	0.022
	(AF)	0.226	0.018	0.237	0.070	0.229	0.049
5d metals							
Ta	(AF)					0.111	-0.266
W	(FM)	0.261	-0.042			0.163	0.002
Re	(FM)	0.517	-0.018	0.506	0.141 <sup>a, <math>\hat{y}</math></sup>	0.504	0.145
Os	(AF)					0.095	-0.160
Ir	(FM)	0.690	0.433				
	(AF)					0.157	0.458
Pt	(AF)					0.139	0.325
Au	(AF)					0.038	0.135

It could be worthwhile to search for the atomic chains in the break-junction experiments using Zr. Finally, the Ir and Pt zigzag chains were reported to have a high-spin to low-spin transition near the local energy minimum.<sup>16,55</sup> In the present studies, the spin magnetic moment for Ir (Zr) in the ladder-like structure is 0.629 (0.162)  $\mu_B/\text{atom}$  but becomes 0.285 (0.295)  $\mu_B/\text{atom}$  in the elongated energy minimum structure. In the W and Re zigzag chains, we found a magnetic to nonmagnetic transition from the first energy minimum to the second energy minimum. For the Nb, Mo, Tc, Pt and Au zigzag chains, both first and second energy minimum states are nonmagnetic, and therefore, no high-spin to low-spin transition occurs.

When the SOC is taken into account, not only the spin magnetic moments would depend on the magnetization direction but also the orbital magnetic moments would appear. In the 3d TM chains, the spin magnetic moments are hardly affected by the SOC<sup>33</sup> because of the smallness of the SOC in these systems. In contrast, in the 5d TM chains, the SOC is so large that it not only would affect the size of the magnetic moments but also could suppress or induce magnetism itself, depending on the magnetization orientation, as mentioned already in Sec. IIIb. The magnetic moments in the magnetic zigzag chains for the magnetization along three coordinate axes from fully relativistic charge self-consistent calculations are listed in

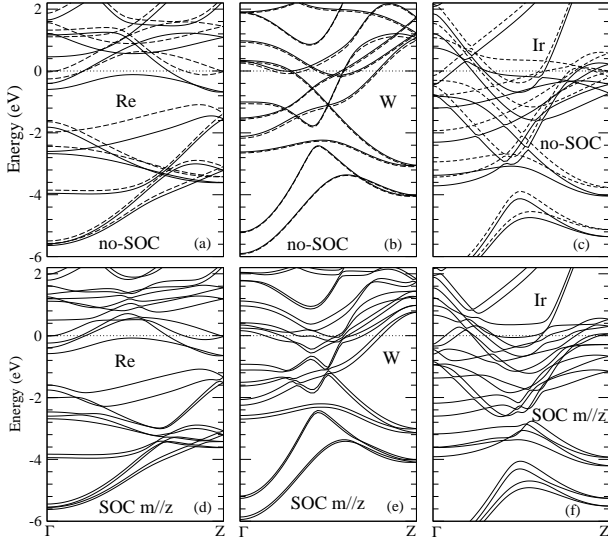


FIG. 8: Scalar-relativistic (a-c) and fully relativistic (d-f) band structures of the Re, W, and Ir zigzag atomic chains in the FM state. In (d-f), the spin magnetization is along the chain direction (i.e., the  $z$ -axis). The Fermi level (the dotted horizontal line) is at the zero energy.

Table V. We notice that all  $5d$  TM chains exhibit the remarkable CMA<sup>45</sup> behavior. Even two  $4d$  (AF Tc and FM Pd) zigzag chains show the CMA too. In particular, in the FM Ir chain, the magnetism occurs only when the magnetization is along the chain. In contrast, in the AF Ir chain, the magnetism appears only when the magnetization is parallel to the  $y$ -axis (Fig. 1b). The orbital magnetic moments in the Zr, Tc, Ru, Rh, Ta, Re, Os, Ir, Pt, Au chains are rather significant ( $\geq 0.1 \mu_B/\text{atom}$ ) (Table V). In the Rh, Ir and Pt zigzag chains, the orbital magnetic moments can be as large as  $0.3 \mu_B/\text{atom}$ . As in the linear chains (Table II), the orbital moments in the zigzag chains depend strongly on the magnetization orientation (Table VI).

### B. Band structures and density of states

The band structures of the FM Re, W and Ir zigzag chains are displayed in Fig. 8, as representatives. Compared with the corresponding band structures of the linear chains (e.g., Ir in Fig. 5), the number of bands become doubled in the zigzag chains because of the doubling of the number of atoms. Furthermore, unlike the linear chains where the  $d_{xy}(d_{xz})$  and  $d_{x^2-y^2}(d_{yz})$  bands (Fig. 5d) are degenerate because of rotational invariance, the  $d_{xy}(d_{xz})$  and  $d_{x^2-y^2}(d_{yz})$  bands are now split because of the strong anisotropy in the  $x-y$  plane perpendicular to the chain axis. It is clear that the energy bands are also highly spin-split and the separation of the spin-up and spin-down bands may be correlated with the spin magnetic moment.

As for the linear chains, we calculate the spin-

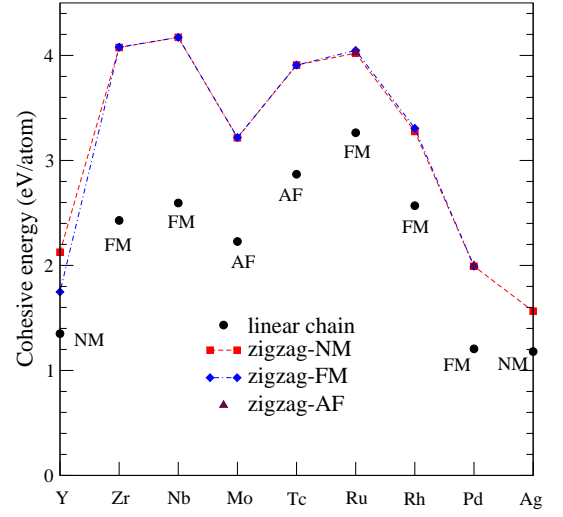


FIG. 9: (color online) The cohesive energy of the  $4d$  TM zigzag chains in the NM, FM and AF states. For comparison, the ground state cohesive energy of the corresponding linear chains is also plotted (solid circles). The ground state magnetic configuration of the linear chains is labelled as NM or FM or AF near each solid circle.

polarization ( $P$ ) and count the numbers of spin-up and spin-down conduction bands at the Fermi level in the FM zigzag chains, as listed in Table III. The  $P$  in the considered zigzag chains generally gets reduced when compared with that in the linear chains (Table III). Nevertheless, the  $P$  of the Rh zigzag chain is as large as 0.53. Interestingly, the sign of the  $P$  in the Zr chain changes from positive to negative when it transforms from the linear to zigzag chain structure.

## V. STABILITY OF LINEAR CHAIN STRUCTURES

Let us now examine the relative stability of the linear and zigzag chains by comparison of the total energies of the two structures. The ground state cohesive energy of the linear chains and the cohesive energies of the zigzag chains in the NM, FM and AF states are displayed in Fig. 9 (for  $4d$  TM) and Fig. 10. (for  $5d$  TM). The cohesive energy ( $E_c$ ) is defined as the difference in the total energy between the free atom ( $E_a$ ) and the chain ( $E_t$ ), i.e.  $E_c = E_a - E_t$ . A positive value of the  $E_c$  means that the formation of the chain from the free atoms would save energy, i.e., the chain would be stable against breaking up into free atoms. The total energies of the free atoms are calculated by the cubic box supercell approach with the cell size of  $15 \text{ \AA}$ . The electronic configurations used for  $4d$  TM are  $4d^1 5s^2$  (Y),  $4d^3 5s^2$  (Zr),  $4d^4 5s^1$  (Nb),  $4d^5 5s^1$  (Mo),  $4d^6 5s^1$  (Tc),  $4d^7 5s^1$  (Ru),  $4d^8 5s^1$  (Rh),  $4d^9 5s^1$  (Pd) and  $4d^{10} 5s^1$  (Ag). And for  $5d$  TM are  $5d^1 6s^2$  (La),  $5d^3 6s^1$  (Hf),  $5d^4 6s^1$  (Ta),  $5d^5 6s^1$  (W),  $5d^6 6s^1$  (Re),  $5d^7 6s^1$  (Os),  $5d^8 6s^1$  (Ir),  $5d^9 6s^1$  (Pt) and  $5d^{10} 6s^1$  (Au).

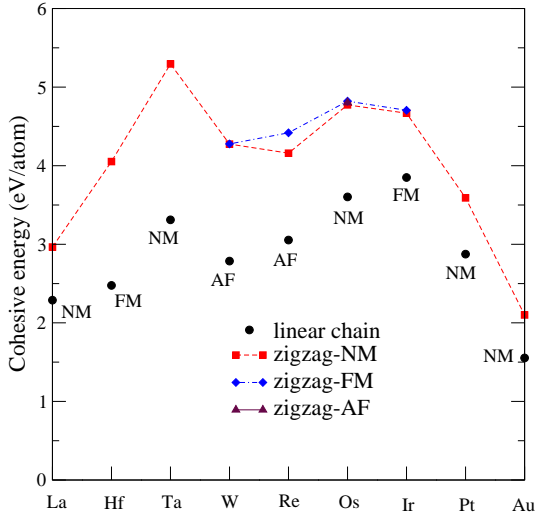


FIG. 10: (color online) The cohesive energy of the 5d TM zigzag chains in the NM, FM and AF states. For comparison, the ground state cohesive energy of the corresponding linear chains is also plotted (solid circles). The ground state magnetic configuration of the linear chains is labelled as NM or FM or AF near each solid circle.

We note that in all cases, the ground state cohesive energy of the linear chain is smaller than that of the zigzag chain (Figs. 9 and 10). This suggests that the 4d and 5d linear chains are unstable against the zigzag structural distortion, as may be expected from the Peierls instability of linear one-dimensional monoatomic metals.<sup>48</sup> The difference in the ground state energy between the linear and zigzag structures for all the 4d and 5d elements is rather large, ranging from 0.8 to 2.0 eV/atom. This shows that the free standing 4d and 5d TM linear chains would not be the stable state, and the linear chains may occur only in constrained conditions such as on the steps on a vicinal surface<sup>4</sup> and under tensile stress in the break-point experiments<sup>8,49–51</sup>. Interestingly, a recent *ab initio* study<sup>52</sup> showed that alloying the gold nanowires with cesium could make linear monoatomic chains stable.

## VI. MAGNETIC ANISOTROPY ENERGY

The total energy as a function of the magnetization orientation  $(\theta, \phi)$  of a 1D wire may be written, in the lowest non-vanishing terms, as

$$E_t = E_0 + \sin^2 \theta (E_1 - E_2 \cos^2 \phi) \quad (2)$$

where  $\theta$  is the polar angle of the magnetization away from the chain axis ( $z$ -axis) and  $\phi$  is the azimuthal angle in the  $x-y$  plane perpendicular to the wire, measured from the  $x$  axis. For the free standing linear atomic chains, the azimuthal anisotropy energy constant  $E_2$  is zero. The axial anisotropy energy constant  $E_1$  is then given by the total energy difference between the magnetization along the  $y(x)$  and  $z$  axes, i.e.,  $E_1 = E^y - E^z$  ( $E^x = E^y$ ). A

TABLE VII: Total ( $E_1^t$ ), electronic ( $E_1^e$ ) and dipolar ( $E_1^d$ ) magnetic anisotropy energies (in meV/atom) of the 4d and 5d transition metal linear chains. If  $E_1^t$  is positive, the easy magnetization axis is along the chain; otherwise, the easy magnetization axis is perpendicular to the chain.

	FM			AF		
	$E_1^t$	$E_1^e$	$E_1^d$	$E_1^t$	$E_1^e$	$E_1^d$
4d metals						
Zr	-0.277	-0.286	0.009			
Mo				-2.783	-2.924	0.141
Tc				7.228	7.186	0.042
Ru	-11.99	-12.03	0.044			
Rh	6.997	6.993	0.004			
Pd	-1.760	-1.770	0.012			
5d metals						
Hf	0.825	0.825	0.000			
W				-5.235	-5.283	0.048
Re				-59.94	-60.01	0.070
Ir	-11.13	-11.14	0.014			

positive value of  $E_1$  means that the chain ( $z$ ) axis is the easy magnetization axis. For the zigzag chains which are in the  $x-z$  plane,  $E_2$  is not zero and can be calculated as the total energy difference between the magnetization along the  $x$  and  $y$  axes, i.e.,  $E_2 = E^y - E^x$ .

The magnetic anisotropy energy for a magnetic solid consists of two contributions. One comes from the magnetocrystalline anisotropy in the electronic band structure caused by the simultaneous occurrence of the electron spin-orbit interaction and spin-polarization in the magnetic system, and *ab initio* calculation of this part has already been described in Sec. II. The other is the magnetostatic (or shape) anisotropy energy due to the magnetic dipolar interaction in the solid. The shape anisotropy energy is zero for the cubic systems such as bcc Fe and fcc Ni, and also negligibly small for weakly anisotropic solids such as hcp Co. However, for the highly anisotropic structures such as magnetic Fe and Co monolayers,<sup>53,54</sup> the shape anisotropy energy can be comparable to the electronic MAE, and therefore cannot be neglected. For the collinear magnetic systems (i.e.  $\mathbf{m}_q/\mathbf{m}_{q'}$ ), this magnetic dipolar energy  $E_d$  is given by (in atomic Rydberg units)<sup>53</sup>

$$E^d = \sum_{qq'} \frac{m_q m_{q'}}{c^2} M_{qq'} \quad (3)$$

where  $M_{qq'}$  is called the magnetic dipolar Madelung constant which is evaluated by Ewald's lattice summation technique<sup>56</sup>. The speed of light  $c = 274.072$ , and  $m_q$  is the atomic magnetic moment on site  $q$  in the unit cell. Note that in atomic Rydberg units, one Bohr magneton ( $\mu_B$ ) is  $\sqrt{2}$ . Therefore, as noted recently in Ref. 33, the  $E_d$  for the multilayers obtained previously by Guo *et al.*<sup>53,54</sup> is too small by a factor of 2.

The calculated  $E^d$ 's for the linear and zigzag chains are listed in Tables VII and VIII, respectively. Tables VII

and VIII show that in both the linear and zigzag chains and in both the FM and AF states, the  $E^d$ 's are much smaller than the electronic contributions ( $E^e$ ), being in strong contrast to the case of the 3d TM chains.<sup>33</sup> This is because the magnetization here is significantly lower and the equilibrium bond length becomes larger, compared with that of the 3d TM chains.<sup>33</sup> Furthermore, they always prefer the chain direction ( $z$  axis) as the easy magnetization axis. Therefore, any perpendicular magnetic anisotropy must originate from the electronic magnetocrystalline anisotropy.

The calculated  $E^e$ 's of the linear and zigzag atomic chains are also listed in Tables VII and VIII, respectively. Table VII shows that in the FM linear chains at equilibrium, the  $E^e$  would favor a perpendicular anisotropy in the Zr, Ru, Pd and Ir chains but prefer the chain axis in the Rh and Hf chains. In the AF state, in contrast, the Mo, W and Re linear chains would have the easy axis perpendicular to the chain while only the Tc linear chain prefer the axial anisotropy. Remarkably, the FM Ru, Rh and Ir as well as AF Tc and Re linear chains have a large total anisotropy energy ( $E^t$ ) (see Table VII) of  $\sim 10$  meV/atom. In particular, the  $E^t$  of the AF Re linear chain is as large as -60 meV/atom. *Ab initio* calculations of the  $E^e$  of the 4d TM linear chains have been reported recently<sup>44</sup>, and our present results for the equilibrium bondlengths (Table VII) agree rather well with these earlier calculations (Fig. 1 in Ref. 44).

The electronic anisotropy energy for the selected linear 4d and 5d atomic chains is displayed as a function of bond length in Fig. 11. It is clear that in several selected linear chains, the magnitude of the  $E^e$  generally increases with the bondlength (Fig. 11a), like the spin and orbital magnetic moments (Fig. 4). For example, the  $E^e$  of the Rh chain increases from 7.0 meV/atom at the equilibrium bondlength (2.25 Å) to 37.3 meV/atom at bondlength of 3.0 Å. Several chains also undergo interesting spin-reorientation transition as the bondlength is elongated.

When elongated, for example, the FM Zr, Nb, Ru, and Ir linear chain would undergo a spin reorientation transition from the perpendicular to along the axial direction at the bondlength of  $\sim 2.75$  Å,  $\sim 2.82$  Å,  $\sim 2.65$  Å, and  $\sim 2.45$  Å, respectively. In contrast, the magnetization of the Ta chain transits from that along the axis to the perpendicular direction at  $\sim 2.85$  Å. Furthermore, many elongated chains have a gigantic anisotropy energy of  $\sim 20$  meV/atom (Fig. 11).

Table VIII shows that the size of the axial anisotropy energy ( $E_1$ ) in the zigzag chains is large and is generally comparable to that in the linear chains (Table VII). However, unlike the linear chains, there is also the pronounced anisotropy ( $E_2$ ) in the  $x-y$  plane perpendicular to the chain axis in many zigzag structures (Table VIII). In the FM Y, AF Ru and Os zigzag chains, the magnitude of the  $E_2^t$  is even larger than that of  $E_1^t$ . In the FM Y, Mo, AF Ru, FM Rh, FM Re, and FM Ir zigzag chains, the easy axis is along the chain direction. In the FM Ru as well as FM and AF Pd chains, the easy axis is perpendicular to

the zigzag plane. In the Zr, W, and Os chains, the easy axis is in the zigzag plane but perpendicular to the chain axis. *Ab initio* calculations for only the Ir and Pt zigzag chains have recently been reported.<sup>16</sup> However, in Ref. 16, the easy axis is reported to be along the  $x$ -axis. This discrepancy may be due to the pronounced difference in the equilibrium zigzag structure between the present and previous calculations. Furthermore, we find the Pt zigzag chain to nonmagnetic.

Structural transformation from the linear to zigzag structure has profound effect on magnetism in the 4d and 5d TM nanowires. This transformation not only induces (or suppresses) magnetization in, e.g., the Y and Os chains (the Tc and Hf chains), as mentioned already in Sec. IV, but also causes spin reorientation transition in, e.g., the Re and Ir chains (Tables VII and VIII). Note that the linear AF Re chain has a gigantic perpendicular anisotropy energy of -60.0 meV/atom (Table VII). However, upon transition to the zigzag structure, the AF state disappears, and, instead, the FM state appears with the magnetization switched to be along the chain axis.

## VII. CONCLUSIONS

We have performed an extensive *ab initio* study of the physical properties of both linear and zigzag atomic chains of all 4d and 5d transition metals within the GGA by using the accurate PAW method. First, the atomic structures were determined. All the TM linear chains are found to be unstable against the corresponding zigzag structures. All the TM chains except Nb, Ag and La, have a stable (or metastable) magnetic state in either the linear or zigzag or both structures. Magnetic states appear also in the Nb and La linear chains when the chains are sufficiently elongated. The spin magnetic moments in the Mo, Tc, Ru, Rh, W, Re chains could be large ( $\geq 1.0 \mu_B$ /atom). Structural transformation from the linear to zigzag chains can suppress the magnetism already in the linear chain, induce the magnetism in the zigzag structure, and also cause a change of the magnetic state (FM to AF or vice versa).

With the SOC included, our calculations show that the orbital moments in the Zr, Tc, Ru, Rh, Pd, Hf, Ta, W, Re, Os, Ir and Pt chains could be rather large ( $\geq 0.1 \mu_B$ /atom). Importantly, large magnetic anisotropy energy ( $\geq 1.0$  meV/atom) is found in most of the magnetic TM chains, suggesting that these nanowires could have important applications in ultrahigh density magnetic memories and hard disks. In particular, giant magnetic anisotropy energy ( $\geq 10.0$  meV/atom) could appear in the Ru, Re, Rh, and Ir chains. Furthermore, the magnetic anisotropy energy in several linear chains could be as large as 40.0 meV/atom when the chains are under sufficiently large tensile strain. A spin-reorientation transition occurs in the Ru, Ir, Ta, Zr, La and Zr, Ru, La, Ta and Ir linear chains when they are elongated. Remarkably, all the 5d as well as Tc and Pd chains show

TABLE VIII: The total ( $E_1^t, E_2^t$ ), electronic ( $E_1^e, E_2^e$ ) and dipolar ( $E_1^d, E_2^d$ ) magnetic anisotropy energy constants (in meV/atom) as well as the easy magnetization axis ( $\mathbf{M}$ ) of the 4d and 5d transition metal zigzag chains.  $E_1 = E^y - E^z$ ;  $E_2 = E^y - E^x$ , see Equ. (2).

	FM						AF							
	$E_1^e$	$E_2^e$	$E_1^d$	$E_2^d$	$E_1^t$	$E_2^t$	M	$E_1^e$	$E_2^e$	$E_1^d$	$E_2^d$	$E_1^t$	$E_2^t$	M
	4d metals													
Y	0.028	-1.925	0.004	0.002	0.032	-1.923	$z$							
Zr	0.000	0.018	0.001	0.000	0.001	0.018	$x$							
Mo	0.009	0.009	0.001	0.000	0.010	0.009	$z$							
Ru	-2.673	-0.084	0.084	0.041	-2.589	-0.043	$y$	0.441	-0.544	0.004	-0.002	0.445	-0.548	$z$
Rh	10.675	3.182	0.059	0.029	10.734	3.211	$z$							
Pd	-0.695	-0.487	0.005	0.002	-0.690	-0.485	$y$	-1.125	-0.860	0.001	-0.001	-1.123	-0.861	$y$
	5d metals													
W	-0.540	0.240	0.002	0.001	-0.538	0.241	$x$							
Re	1.062	1.043	0.008	0.004	1.070	1.047	$z$							
Os	-9.402	0.319	0.007	0.004	-9.395	0.323	$x$	-4.798	5.340	0.002	-0.002	-4.796	5.338	$x$
Ir	17.595	-6.430	0.014	0.006	17.609	-6.424	$z$							

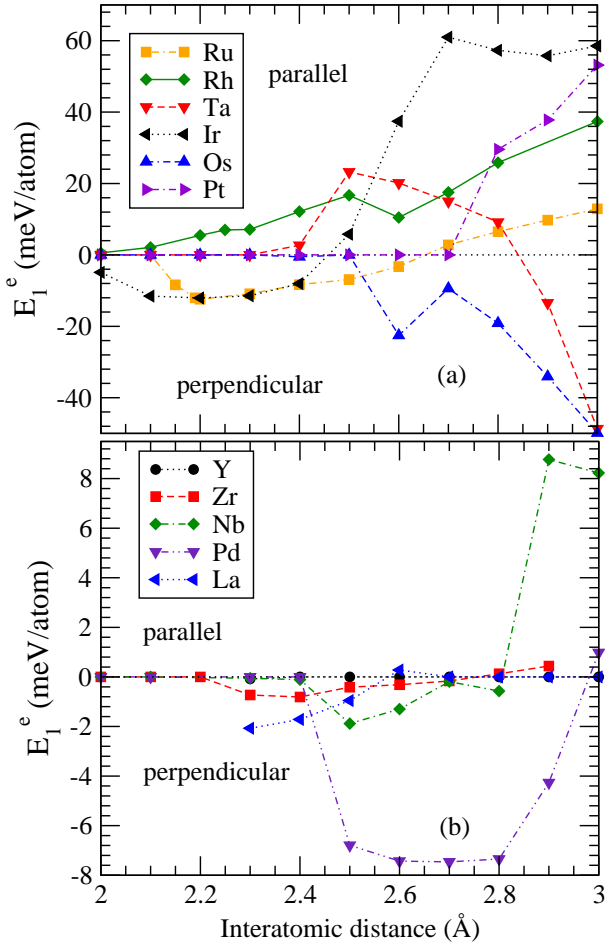


FIG. 11: (color online) Magnetocrystalline anisotropy energy ( $E_1^e$ ) of the selected 4d and 5d transition metal linear atomic chain as a function of interatomic distance. The upper panels contains the TM linear chain with larger MAE. A positive value of  $E_1^e$  means that the magnetization would be parallel to the chain axis whilst a negative value would mean that the easy magnetization axis would be perpendicular to the chain.

the fascinating behavior of the so-called colossal magnetic anisotropy.<sup>45</sup> Finally, the electronic band structure and density of states of the nanowires have also been calculated mainly in order to understand the electronic origin of the large magnetic anisotropy and orbital magnetic moment as well as to calculate the conduction electron spin polarization.

## VIII. ACKNOWLEDGEMENTS

The authors acknowledge supports from National Science Council and NCTS of Taiwan. They also thank National Center for High-performance Computing of Taiwan and NTU Computer and Information Networking Center for providing CPU time.

- <sup>1</sup> H. J. Elmers, J. Hauschild, H. Höche, U. Gradmann, H. Bethge, D. Heuer, and U. Köhler, Phys. Rev. Lett. **73**, 898 (1994).
- <sup>2</sup> S. Heinze, M. Bode, A. Kubetzka, O. Pietzsch, X. Nie, S. Blügel, and R. Wiesendanger, Science **288**, 1805 (2000)
- <sup>3</sup> O. Pietzsch, A. Kubetzka, M. Bode, and R. Wiesendanger, Phys. Rev. Lett. **84**, 5212 (2000)
- <sup>4</sup> P. Gambardella, A. Dallmeyer, K. Maiti, M. C. Malagoli, W. Eberhardt, K. Kern C. Carbone, Nature **416**, 301 (2002).
- <sup>5</sup> D. Li, B. R. Cuenya, J. Pearson, S. D. Bader, and W. Kuene, Phys. Rev. B **64**, 144410 (2001).
- <sup>6</sup> S. B. Suh, B. H. Hong, P. Tarakeshwar, S. J. Youn, S. Jeong, and K. S. Kim, Phys. Rev. B **67**, 241402(R) (2003).
- <sup>7</sup> G. Rubio, N. Agrait, and S. Vieira, Phys. Rev. Lett. **76**, 2302 (1996).
- <sup>8</sup> V. Rodrigues, J. Bettini, P. C. Silva and D. Ugarte, Phys. Rev. Lett. **91**, 096801 (2003)
- <sup>9</sup> A. Dallmeyer, C. Carbone, W. Eberhardt, C. Pampuch, O. Rader, W. Gudat, P. Gambardella, and K. Kern, Phys. Rev. B **61**, R5133 (2000)
- <sup>10</sup> J. Hong and R. Q. Wu, Phys. Rev. B **67**, 020406(R) (2003)
- <sup>11</sup> C. Ederer, M. Komelj, and M. Fahnle, Phys. Rev. B **68**, 052402 (2003)
- <sup>12</sup> B. Lazarovits, L. Szunyogh, and P. Weinberger, Phys. Rev. B **67**, 024415 (2003).
- <sup>13</sup> M. Komelj, C. Ederer, J. W. Davenport, and M. Fahnle, Phys. Rev. B **66**, 140407(R) (2002).
- <sup>14</sup> D. Spisak, and J. Hafner, Phys. Rev. B **65**, 235405 (2002).
- <sup>15</sup> D. Spisak, and J. Hafner, Phys. Rev. B **67**, 214416 (2003).
- <sup>16</sup> L. Fernández-Seírvane, V. M. García-Suárez, and J. Ferrer, Phys. Rev. B **75**, 075415 (2007).
- <sup>17</sup> F. J. Ribeiro, and M. L. Cohen, Phys. Rev. B **68**, 35423 (2003).
- <sup>18</sup> T. Nautiyal, S. J. Youn, and K. S. Kim, Phys. Rev. B **68**, 033407 (2003).
- <sup>19</sup> S. R. Bahn and K. W. Jacobsen, Phys. Rev. Lett. **87**, 266101 (2001).
- <sup>20</sup> A. Delin, and E. Tosatti, Phys. Rev. B **68**, 144434 (2003).
- <sup>21</sup> N. V. Skorodumova, and S. I. Simak, Comput. Mater. Sci. **17**, 178 (2000).
- <sup>22</sup> L. D. Maria, and M. Springborg, Chem. Phys. Lett. **323**, 293 (2000).
- <sup>23</sup> Y.-S. Lin, A.-Y. Li, and Z.-Z. Zhu, Chin. Phys. Lett. **21**, 1791 (2004).
- <sup>24</sup> D. Sanchez-Portal, E. Artacho, J. Junquera, P. Ordejon, A. Garcia, and J. M. Soler, Phys. Rev. Lett. **83**, 3884 (1999).
- <sup>25</sup> D. Sanchez-Portal, E. Artacho, J. Junquera, A. Garcia, and J. M. Soler, Surf. Sci. **482** – **485**, 1261 (2001).
- <sup>26</sup> T. Nautiyal, T. H. Rho, and K. S. Kim, Phys. Rev. B **69**, 193404 (2004).
- <sup>27</sup> Z.-Z. Zhu, J.-C. Zheng, and G. Y. Guo, Chem. Phys. Lett. **472**, 99 (2009).
- <sup>28</sup> J. Hong, Phys. Rev. B **73**, 092413 (2006).
- <sup>29</sup> Y. Mokrousov, G. Bihlmayer, and S. Blügel, Phys. Rev. B **72**, 045402 (2005).
- <sup>30</sup> G. Autes, C. Barreteau, D. Spanjaard and M.-C. Desjonqueres, J. Phys.: Condens. Matter **18**, 6785 (2006).
- <sup>31</sup> R. Druzinic and W. Hubner, Phys. Rev. B **55**, 347 (1997).
- <sup>32</sup> J. Dorantes-Davila and G. M. Pastor, Phys. Rev. Lett. **81**, 208 (1998).
- <sup>33</sup> J. C. Tung and G. Y. Guo, Phys. Rev. B **76**, 094413 (2007).
- <sup>34</sup> A. J. Heinrich, J. A. Gupta, C. P. Lutz, and D. M. Eigler, Science **306**, 466 (2004).
- <sup>35</sup> P. E. Blöchl, Phys. Rev. B **50**, 17953 (1994); G. Kresse and D. Joubert, *ibid.* **59**, 1758 (1999).
- <sup>36</sup> G. Kresse and J. Hafner, Phys. Rev. B **48**, 13115 (1993).
- <sup>37</sup> G. Kresse, and J. Furthmüller, Comp. Matter. Sci. **6**, 15 (1996).
- <sup>38</sup> Y. Wang and J. P. Perdew, Phys. Rev. B **44**, 13298 (1991); J. P. Perdew and Y. Wang, Phys. Rev. B **45**, 13244 (1991).
- <sup>39</sup> G. H. O. Daalderop, P. J. Kelly, and M. F. H. Schuurmans, Phys. Rev. B **41**, 11919 (1990).
- <sup>40</sup> G. Y. Guo, W. M. Temmerman, and H. Ebert, Phys. Rev. B **172**, 61 (1991).
- <sup>41</sup> The VASP Guide (<http://cms.mpi.univie.ac.at/VASP/>).
- <sup>42</sup> A. Delin, E. Tosatti, and R. Weht, Phys. Rev. Lett. **92**, 057201 (2004).
- <sup>43</sup> A. Delin, E. Tosatti, and R. Weht, Phys. Rev. Lett. **96**, 079702 (2006).
- <sup>44</sup> Y. Mokrousov, G. Bihlmayer, S. Heinze, and S. Blügel, Phys. Rev. Lett. **96**, 147201 (2006).
- <sup>45</sup> A. Smogunov, A. Dal Corso, A. Delin, R. Weht and E. Tosatti, Nat. Nanotech. **3**, 22 (2008).
- <sup>46</sup> H. Takayama, K.-P. Bohnen, and P. Fulde, Phys. Rev. B **14**, 2287 (1976).
- <sup>47</sup> L. J. Whitman, J. A. Stroschio, R. A. Dragoest, and R. J. Celotta, Phys. Rev. Lett. **66**, 1338 (1991).
- <sup>48</sup> C. Kittel, *Introduction to Solid State Physics*, 7th ed. (Wiley, New York, 1996).
- <sup>49</sup> V. Rodrigues, T. Fuhrer, and D. Ugarte, Phys. Rev. Lett. **85**, 4124 (2000).
- <sup>50</sup> J. Guo, Y. Mo, E. Kaxiras, Z. Zhang, and H. H. Weitering, Phys. Rev. B **73**, 193405 (2006).
- <sup>51</sup> S. Shiraki, H. Fujisawa, M. Nantoh, and M. Kawai, Surface Science **552**, 243-250 (2004).
- <sup>52</sup> Y. C. Choi, H. M. Lee, W. Y. Kim, S. K. Kwon, T. Nautiyal, D.-Y. Cheng, K. Vishwanathan, and K. S. Kim, Phys. Rev. Lett. **98**, 076101 (2007).
- <sup>53</sup> G. Y. Guo, W. M. Temmerman, and H. Ebert, J. Phys.: Condens. Matter **3**, 8205 (1991).
- <sup>54</sup> G. Y. Guo, J. Magn. Magn. Mater. **176**, 97-110 (1997).
- <sup>55</sup> V. M. G-Suárez, D. Zs. Manrique, C. J. Lambert, and J. Ferrer, Phys. Rev. B **79**, 060408R (2009).
- <sup>56</sup> P. Ewald, Ann. Phys. **64**, 253 (1921)